A Versatile Silica Functionalization Strategy for Nanomaterials

Keisuke Nagao, Katherine Lei, Peyton Worthington, Noah Kent, Michika Onoda, Elian Malkin, Emmanuel Vargas Paniagua, Rebecca Leomi, Robert J. Macfarlane, and Polina Anikeeva**

K. Nagao, K. Lei, Michika Onoda, R. J. Macfarlane, P. Anikeeva
Department of Materials Science and Engineering
Massachusetts Institute of Technology
Cambridge, MA 02139, USA
E-mail: anikeeva@mit.edu, rmacfarl@mit.edu

K. Nagao, N. Kent, E. Malkin, E. Vargas Paniagua, R. Leomi, P. Anikeeva
Research Laboratory of Electronics and McGovern Institute for Brain Research
Massachusetts Institute of Technology
Cambridge, MA 02139, USA

P. Worthington
Department of Mechanical Engineering
Massachusetts Institute of Technology
Cambridge, MA 02139, USA

E. Malkin, P. Anikeeva
Department of Brain and Cognitive Sciences
Massachusetts Institute of Technology
Cambridge, MA 02139, USA

M. Onoda
Pure Lithium
Charlestown, MA 02129, USA

Keywords: silica shell coating, reverse microemulsion method, magnetic nanoparticles, nanodiscs, quantum dots

Abstract

Chemical interactions between nanoparticles and their surroundings are governed by their surface chemistry, and thus a versatile strategy for surface functionalization compatible with a variety of particle compositions would empower nanotechnology research. Although silica coating offers a promising approach, common protocols are often impeded by inconsistent reproducibility, non-uniform thicknesses, difficulty in producing thin coatings, and particle aggregation during functionalization. Here, we demonstrate that these challenges can be overcome by adding additional surface ligands to stabilize the particle cores during the silica growth process. The inclusion of excess ligands alters the nanoparticles' surface chemistry such that particle aggregation is suppressed, even for thin silica coatings (<1 nm) and coatings on a wide range of nanoparticle compositions, sizes, and shapes. The versatility and reproducibility of this approach is illustrated through its application to isotropic magnetite nanoparticles with diameters between 20-28 nm, anisotropic magnetite nanodiscs >200 nm in diameter, and CdS/ZnS quantum dots. These silica-coated nanomaterials retain their functional properties, and the silica shell can be further modified with application-specific organic moieties. Being agnostic to the nanomaterials shape and composition, this approach is enabling to nanomaterials applications demanding precise control over their surface chemistry independent of their functional properties.

1. Introduction

Controlling the surface properties of solution-dispersed nanomaterials is vital for ensuring their stability, processability, and uniformity in properties and functions.[1,2] These factors are particularly important for their applications in biological environments.[3] It is not uncommon for a nanomaterial with promising physical properties to be toxic without the appropriate surface chemistry.[4–13] Furthermore, biomedical applications of nanomaterials often require functionalization with moieties that target specific cells or molecules.[14,15]

The diversity of compositions, geometries, and dimensions that gives rise to innumerable functional properties in nanomaterials also poses a formidable challenge to engineering of their surface properties, which often manifests in reinventing the functionalization procedures for each nanomaterial. The encapsulation of nanomaterials with thin silica shells presents a promising solution for surface modification, since silica is biochemically inert and readily lends itself to further functionalization.[16–20] Although several silica coating methods have been developed, the reverse microemulsion method (RMM) is the primary procedure used to silica-coat nanomaterials with hydrophobic surfaces.[11,21–25] The RMM method involves the exchange of nanoparticles' hydrophobic ligands with hydrolyzed tetraethyl orthosilicate (TEOS) and subsequent phase transfer from non-polar solvents to reverse water micelles, where silica shells grow on nanomaterials. Since many types of nanomaterials are produced in organometallic colloidal syntheses that yield hydrophobic surface ligands, commonly oleylamine or oleic acid (OAc), RMM is applicable to a wide range of colloidal nanoparticles.[26,27]

Despite its utility, RMM often has challenges in reproducibility, as protocols often need to be adapted for each new particle composition being examined. Common failure modes are the production of empty silica spheres alongside the silica coated particles, or the aggregation of particles during coating to produce large, multicore silica-coated clusters (**Figure 1a**). Thus, multiple RMM procedures have been published for the coating of different nanoparticle

composition, each containing variations in both reagent composition and reaction protocols. These investigations have significantly advanced this area of research, and disparate design rules have been proposed to avoid the formation of empty silica spheres, such as matching the number of nanoparticles with reverse micelles or adjusting the total surface area of nanoparticles.[22,28] Additionally, modifications such as the addition of excess surfactants or pre-treatment of particles to alter their ligand shell conformations have shown benefits in reducing either the number of empty silica spheres or the formation of multicore clusters. However, even with these advancements, it can still be challenging to reliably reproduce prior protocols when they are performed in new research environments or applied to novel particle compositions. Even with time-consuming optimization efforts to adapt protocols to emerging nanomaterials chemistries, multi-core particles often form easily and thereby change the balance between the number of nanoparticles and reverse micelles, breaking the design rules. A robust and straightforward strategy to simplify the process of adapting these useful and beneficial RMM silica coating approaches would minimize current bottlenecks in colloidal surface functionalization.

We hypothesized that the poor reproducibility of many RMM methods stems from the significant variation in the initial surface state of the particles being coated. Specifically, the ligands (e.g. OAc) used to stabilize these particles in a colloidal suspension bind to the particle surface dynamically, and thus the chemical reactions occurring during the silica growth process likely perturb the surface composition of the particles. As a result, much of the difficult in replicating RMM protocols or translating them to new particle compositions may stem from the manner in which these differences affect ligand coatings during the RMM process. Although secondary co-surfactants have been used to alter the properties of micelles in previous RMM protocols, these surfactants typically do not contain functional groups that bind strongly to the particles' surfaces.[29] Thus, while these prior surfactants may alter the composition of the micelles surrounding the hydrophobic ligand-grafted particles, they are not anticipated to

significantly alter the composition of the ligand shell itself. We therefore hypothesized that the incorporation of additional OAc directly to the silica shell coating solution would ensure that the ligand coating of nanomaterials remain saturated during RMM regardless of particle type, size, synthesis protocol, and particle batch.[23,25] Here we demonstrate that the inclusion of additional ligand (as opposed to additional surfactant) allows nanomaterials enter the reverse micelles individually, resulting in almost exclusively single-core particles. As the formation of multi-core aggregates is prevented, established design rules, such as number-based matching of the number of nanomaterials and reverse micelles, give one-to-one core-shells without the emergence of core-free silica spheres. This new, robust method, termed SCHLR (Silica Coating with Hydrophobic Ligands in Reverse microemulsion), consistently produces uniform silica coatings on nanomaterials independent of their core chemistry or the integrity of their organic surface passivation.

Notably, the SCHLR method offers the formation of shells with thickness under 1 nm, which was previously unattainable with RMM methods due to aggregation of nanomaterials.[30,31] SCHLR can be applied to a variety of sizes and compositions of nanomaterials, and can be subsequently followed with a wealth of robust silica-functionalization chemistries to link organic targeting moieties. The SCHLR method therefore holds promise as a facile, reproducible, and universal method for silica shell coating of nanomaterials.

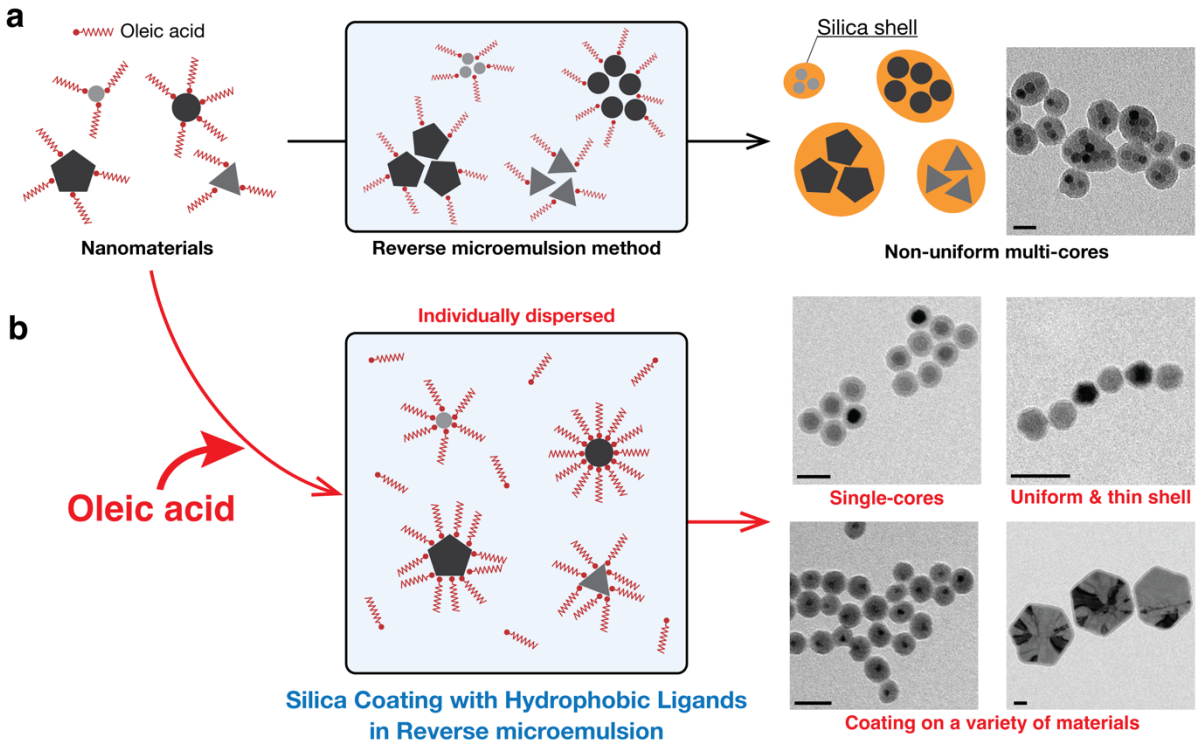

Figure 1. (a) Illustration of challenges in silica coating of nanomaterials via RMM. **(b)** Illustration of silica shell coating via Silica Coating with Hydrophobic Ligands in Reverse microemulsion (SCHLR) that is reproducible and agnostic toward nanomaterial core chemistry, size, or geometry. Scale bars, 50 nm.

2. Results and Discussion

OAc is commonly used as a ligand for nanoparticles to preserve their colloidal stability and prevent agglomeration. We therefore hypothesized that OAc-capped nanomaterials aggregate during the reverse microemulsion silica shell formation reaction when their surfaces are not fully passivated with OAc (due to particle storage or purification steps between their synthesis and coating). Introducing OAc into the silica shell coating solution was expected to facilitate particles separation from each other and prevent the formation of multi-core assemblies. Note that because OAc can also act as a surfactant, it was not initially obvious that its inclusion would not negatively affect the micelles critical to the RMM approach.[32–34]

To examine the effects of adding OAc ligand to the RMM solution, we first applied a silica coating RMM to spherical Fe_3O_4 magnetic nanoparticles (MNPs) 24 nm in diameter, produced via a common organometallic synthesis that uses OAc for surface passivation (**Figure 2a 'MNP**

24 nm', S1).[26,35] When these MNPs were directly incorporated into a previously reported RMM, the products comprised <20% single-core particles, and the silica shells exhibited large variations in thickness (**Figure 2a '-OAc', 2d**). In contrast, when the same protocol and reagents were used, but extra OAc (31.5 mM) was added to the coating solution, the emulsion method produced >90% single-core particles with uniform shell thicknesses as corroborated by transmission electron microscopy (TEM) (**Figure 2a '+OAc', 2b, S2**). The difference in hydrodynamic diameter was also confirmed by dynamic light scattering (DLS) (**Figure 2c**). These outcomes were consistent across different batches of MNPs and could be independently reproduced by multiple researchers (**Figure S3**).

Importantly, the prevention of multicore formation was observed over a broad range of OAc additions (6.3 to 75.6 mM OAc). At the lowest concentration, >90% of particles possessed a single MNP per particle, and the fraction of single-cores increased concomitantly with the amount of added OAc. These results are consistent with the hypothesis that additional OAc ensures that all particle surfaces remain saturated with ligand during the silica coating, thereby preventing aggregation (**Figure 2d**). Moreover, they suggest that this method may simplify the process of adapting the RMM to different particle coatings (*vide supra*), given that the concentration of OAc did not need to be precisely calibrated to prevent multi-core formation. However, we observed an upper bound to OAc addition that must be considered in using the SCHLR approach, as the addition of 113 mM OAc failed to produce silica-coated particles (Figure S4). We hypothesize that this failure to coat the particles is due to of the large amount of hydrophobic ligands in the reaction solution affecting the kinetics of ligand exchange necessary for TEOS to bind to the particle surface and produce a silica coating.[25] This observation is also consistent with the hypothesis that the dynamic nature of OAc binding plays a role in the stability of particles during RMM, and with the observations of prior RMM investigations.[25] For example, Koole et al. observed that CdSe quantum dots embedded in silica were similarly not encapsulated above a critical concentration of an added ligand

(dodecanethiol).[25] While this large excess of OAc did impair the silica coating process, our data still indicate that there is a wide range of [OAc] that prevent particle agglomeration during RMM without impairing the silica growth process, indicating that SCHLR is a versatile and straightforward modification to improve silica coating methods.

The effect of OAc on colloidal stability of core particles was further investigated by measuring the nanoparticle hydrodynamic diameter during the silica coating reaction. We observed immediate aggregation upon preparation of the reaction solution (**Figure 1e**). In the absence of OAc, the hydrodynamic diameter only exhibited modest changes in the 600-800 nm range even after 24 h. In contrast, in the presence of 17 mM oleic acid, the hydrodynamic diameter decreased to approximately 50 nm after 7 to 9 h, even though initial aggregation behavior was similar to control conditions without excess OAc. This indicates that OAc individualizes MNPs not in the continuous organic phase (cyclohexane) but upon transfer from cyclohexane to the water reverse micelles, thus preventing multi-core formation.

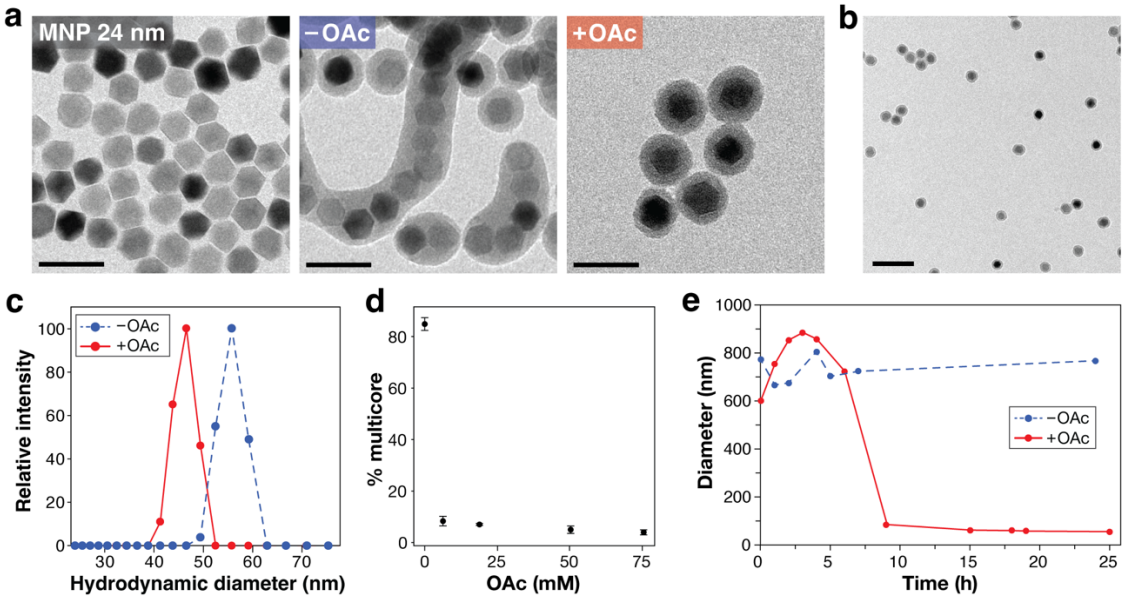

Figure 2. **(a)** TEM images of various silica-coated nanomaterials. The images display bare 24 nm MNPs (left), silica-coated nanomaterials through RMM (middle, labeled '-OAc'), and those produced through the SCHLR method (right, labeled '+OAc'). Scale bars, 50 nm. **(b)** Low magnification TEM image of the same silica-coated MNPs shown in **a "+OAc**'. Scale bar is 100 nm. **(c**) The hydrodynamic diameters of silica-coated 24 nm MNPs measured by dynamic light scattering (DLS). The MNPs were coated using either the conventional method ('-OAc') or the SCHLR method ('+OAc'). **(d)** The relation between the concentration of OAc and proportion of multi-core particles. **(e)** The change in hydrodynamic diameter during the silica shell coating process with ('+OAc') and without oleic acid ('-OAc'), as measured by DLS.

To test the versatility of the SCHLR method, we applied it to nanoparticles of different dimensions, shapes, and compositions. Initially, isotropic Fe_3O_4 MNPs of varying core diameters (20 and 28 nm) were coated using the standard RMM without the addition of OAc to the RMM solution; these MNPs formed multi-core particles and the thickness of the shells were inhomogeneous (**Figure 3a, b "-OAc"**). In contrast, when these MNPs were coated through the SCHLR method (**Figure 3a, b "+OAc", S2**), homogeneous shells were formed and minimal multicore particles were observed. When the SCHLR method was applied to colloidal CdS/ZhS core-shell quantum dots (QDs, d = 11.5 nm, photoluminescence peak, PL, $\boldsymbol{\lambda}_{PL}$ = 650 nm), it produced single-cored, uniformly coated particles (**Figure 3c '+OAc'**). As with the small ferrite nanoparticles, RMM without OAc produced predominantly multicore aggregates (**Figure 3c '-OAc'**). Larger Fe_3O_4 magnetic nanodiscs (MNDs, 240±23.2 nm in diameter, 28.2±3.87 nm thickness) were also coated with silica through the SCHLR method (**Figure 3d 'MND'**). Again, the addition of OAc to RMM yielded uniform silica shells on isolated MNDs (**Figure 3d '+OAc'**). In contrast, in the absence of OAc, the RMM protocol was ineffective, leaving MNDs uncoated and promoting the nucleation of small silica spheres (**Figure 3d '-OAc'**). We hypothesize that in addition to improving the colloidal stability of MNDs, OAc is affecting the size of the reverse micelles and the fluidity of surfactants that comprise the micellar coating, as a 240 nm MND is too large to be encompassed in a typical Igepal-H_2O reverse micelle, (~45 nm under solution conditions examined here).[36] In the absence of OAc, MNDs do not enter

the reverse micelles, which precludes their coating with silica and results in the formation of empty silica spheres seen in the TEM images (**Figure 3d '-OAc'**). These findings indicate SCHLR is broadly applicable to OAc-capped nanoparticles regardless of size, shape, and composition by individualizing nanomaterials upon phase transfer from the oil to water and altering the properties of reverse micelles.

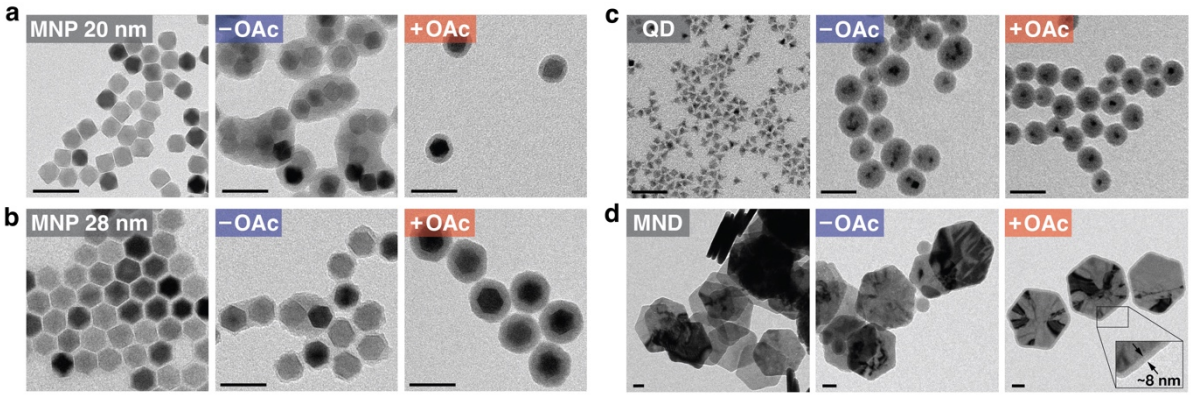

Figure 3. TEM images of various silica-coated 20-nm MNP (**a**), 28-nm MNP (**b**), quantum dots (**c**), and magnetic nanodiscs (**d**). The images display bare nanomaterials (left), silica-coated nanomaterials through RMM (middle, labeled '-OAc'), and those produced through the SCALR method (right, labeled '+OAc'). The synthesis conditions for each panel can be found in Table S2. Scale bars, 50 nm.

In addition to broad nanoparticle composition applicability, the SCHLR method enables precise control over silica-shell thickness. By altering the amount of silica precursor (TEOS), the shell thickness can be linearly tuned between 0.7 nm to 7.7 nm (**Figure 4a, b**). In contrast, in a standard RMM, precisely controlling silica shell thickness was not possible due to the formation of uneven shells and multi-core particles, especially for larger cores or thinner silica shells.[30,31] Yang *et al.* hypothesized that the repulsion force between negatively charged hydrophilic nanomaterials is screened by NH_4^+ at a lower concentration of TEOS, leading to the agglomeration of nanomaterials and the formation of multi-core particles.[31] We anticipate that a similar mechanism might be occurring in the SCHLR method. We hypothesize that additional OAc slows the ligand exchange between OAc and TEOS, which allows more hydrolyzed TEOS

molecules to accumulate in reverse micelles, thereby weakening the electrostatic screening effect. As a result, after the first nanoparticle enters a reverse micelle, the electrostatic interactions between it and other negatively charged nanoparticles are not screened well, which effectively prevents the entry of another particle into the same micelle.

Silica shell thickness was also observed to correlate to the concentration of OAc. Between OAc concentrations of 5 and 45 mM, the silica shell thickness was inversely correlated with the amount of OAc in solution (**Figure 4c, d**). No further decrease in shell thickness was observed above OAc concentrations of 45 mM, but silica coating syntheses at higher OAc concentrations also produced silica nanospheres (~5 nm) devoid of nanoparticle cores (**Figure 4c**). These silica spheres were more numerous at the highest concentrations of OAc. We hypothesize that the addition of extra OAc molecules leads to the formation of small reverse micelles that are composed mainly of OAc molecules that are incapable of incorporating a large nanoparticle. Hydrolyzed TEOS intermediates within these OAc reverse micelles therefore form core-free silica nanospheres. As a result, a portion of the added TEOS is consumed by the formation of silica nanospheres, and the TEOS molecules available to coat nanomaterials decreases, resulting in the thinner shells. Silica nanospheres were not observed at smaller OAc concentrations, at which the formation of multi-core is suppressed (**Figure 1d**). Notably, unlike prior methods that produced silica spheres of comparable size to the coated nanoparticles, these silica spheres are significantly smaller than the coated nanoparticles and thus can be more readily removed from the sample during subsequent purification steps after functionalization of the silica surface with aminoethylaminopropyltrimethoxysilane as discussed below (**Figure 4c "68mM purified").**

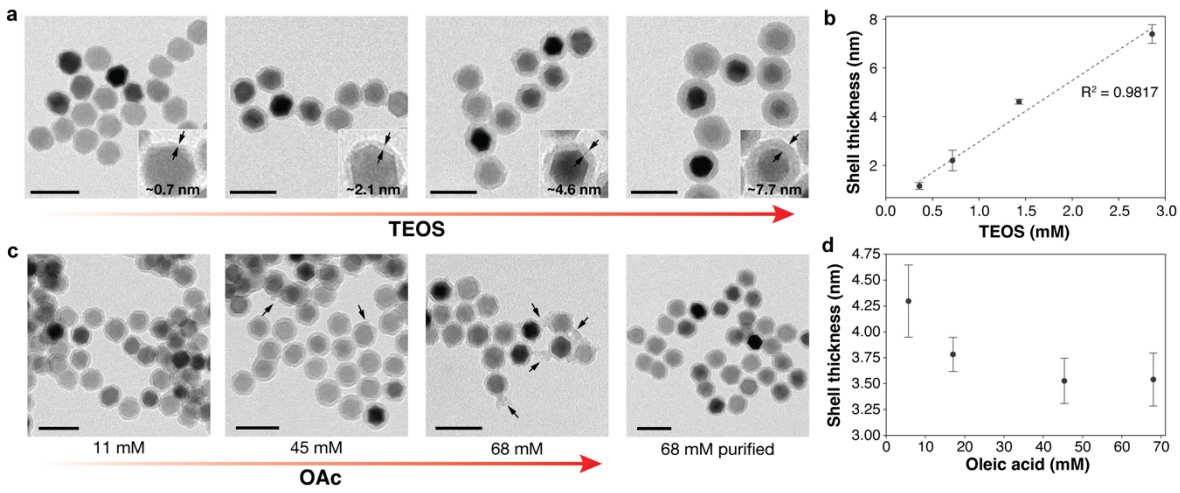

Figure 4. **(a)** TEM images of silica-coated MNPs by SCHLR with different amounts of TEOS. **(b)** The relation between shell thickness and the amount of TEOS (N=3). **(c)** TEM image of silica-coated MNPs at an OAc concentration of 11, 45, and 68 mM. More silica nanospheres (~58 nm) were observed with the amount of OAc added. After purification steps, these silica nanospheres were washed away and no such spheres were observed ("68 mM purified"). (**d**) The relation between shell thickness and concentration of OAc (N=3). The concentration of TEOS was 0.72 mM. Scale bars, 50 nm.

Coating the particles with silica via the SCHLR method does not impair the properties of the nanoparticle cores. For the MNPs, the deposition of silica did not degrade the saturation magnetization (M_s) with the exception of particularly thick (7.6 nm) shells, for which 27 % decrease in M_s was observed (**Figure 5a, b**). This is likely due to partial degradation of MNP cores at large (~3 mM) TEOS concentrations. This is supported by the observation of iron oxide nanodiscs dissolution at TEOS concentrations ~10 times greater (36 mM) than those used for silica-shell deposition (**Figure S5**). In control samples where MNPs were silica-coated in the absence of OAc, a coercivity increase was observed due to aggregation of particles. The formation of multi-core MNP structures causes uniaxial shape anisotropy that scales with the number of particles (**Figure S6**).

One of the most common applications of MNPs is in magnetic hyperthermia, and the efficiency of the MNPs' hysteretic heat dissipation in alternating magnetic fields (AMFs) is measured by the specific loss power (SLP in $W/g_{[Fe]}$).[37] SLP was measured at an AMF with a frequency of

165 kHz and amplitudes of 26 and 35 kA/m (**Figure 5c**). For the low-amplitude AMF condition, SLPs were higher for the MNPs coated with 0.7 nm shells via SCHLR than for the MNPs coated via RMM without the OAc. The SLP of the MNPs coated with thick shells was significantly reduced, which can be attributed to the smaller M_s. At high-amplitude AMF condition, all SLP values increased as expected from the amplitude approaching the coercive field of the particles.[35] Notably, SLPs were higher for the MNPs silica-coated in the absence of OAc. This is consistent with vibrating-sample magnetometer (VSM) measurements that reveal the higher coercivity of multi-core particles (-OAc) as compared to single-core particles (+OAc), which manifests in larger hysteresis loop area. Since the SLP is proportional to the frequency-integrated hysteresis loop area, the difference in heating between –OAc and +OAc is attributed to the ability of the higher (35 kA/m), but not lower (26 kA/m), AMF amplitude to access this entire area.[38]

In addition to magnetic behaviors of MNPs, the spectral characteristics of QDs were measured before and after silica shell coating via SCHLR (**Figure 5d, S7**). The photoluminescence (PL) spectra were nearly identical with no noticeable degradation or peak shift. The quantum yield (ε) after silica shell coating by SCHLR (ε = 0.47) was comparable to polymer-coated QDs (ε = 0.53). In contrast, a notable degradation in quantum yield was observed when the RMM was used (ε = 0.35).

A uniform surface coating for nanomaterials enables standardization of functionalization protocols to alter their surface chemistry. To demonstrate that the SCHLR method empowers such surface modification, silica shell coated MNPs were functionalized with primary amine groups by the addition of [3-(2-aminoethylamino)propyl]trimethoxysilane (AEAPTMS) via commonly used protocols.[19] After purification, these amine-functionalized silica-coated MNPs were labeled with fluorescent dyes through carbodiimide chemistry (**Figure 5e**). Three different dyes, Pacific Blue (PB), Alexa Fluor 488 (AF488), and Alexa Fluor 568 (AF568) with distinct PL excitation and emission profiles (($\boldsymbol{\lambda}_{ex}$, $\boldsymbol{\lambda}_{em}$) = (410, 455 nm), (490, 525 nm), and

(568, 610 nm)) were linked to MNP surfaces. Each of these dyes maintained their PL characteristics after attachment to the silica-coated MNPs, demonstrating that SCHLR coats nanoparticles in functional surfaces that can be directly incorporated into widely applied functionalization protocols.

To further demonstrate the utility of the SCHLR process in engineering nanomaterial surfaces, we modified silica-coated QDs with moieties that permitted their genetic targeting to cells via SNAP-tag® technology that uses a covalent bonding between O^6-benzylguanine (BG) and a SNAP-tag protein (**Figure 5f**).[39] This robust and selective approach is commonly employed in biomedical sciences to deliver non-genetic payloads with genetic specificity. Silica-coated QDs were modified with a combination of BG and polyethylene glycol (PEG) via carbodiimide chemistry (QD-PEG/BG). The addition of PEG ensured colloidal stability of BG-functionalized QDs, minimizing non-specific interactions with HEK293 cells, which were chosen as a widely used mammalian cell line. Following incubation with QD-PEG/BG, HEK293 cells expressing SNAP-tag exhibited significant membrane fluorescence, indicative of specific QD binding, while in the absence of SNAP tag or following incubation with QD-PEG lacking BG moiety negligible membrane fluorescence was observed (**Figure 5f, g**).

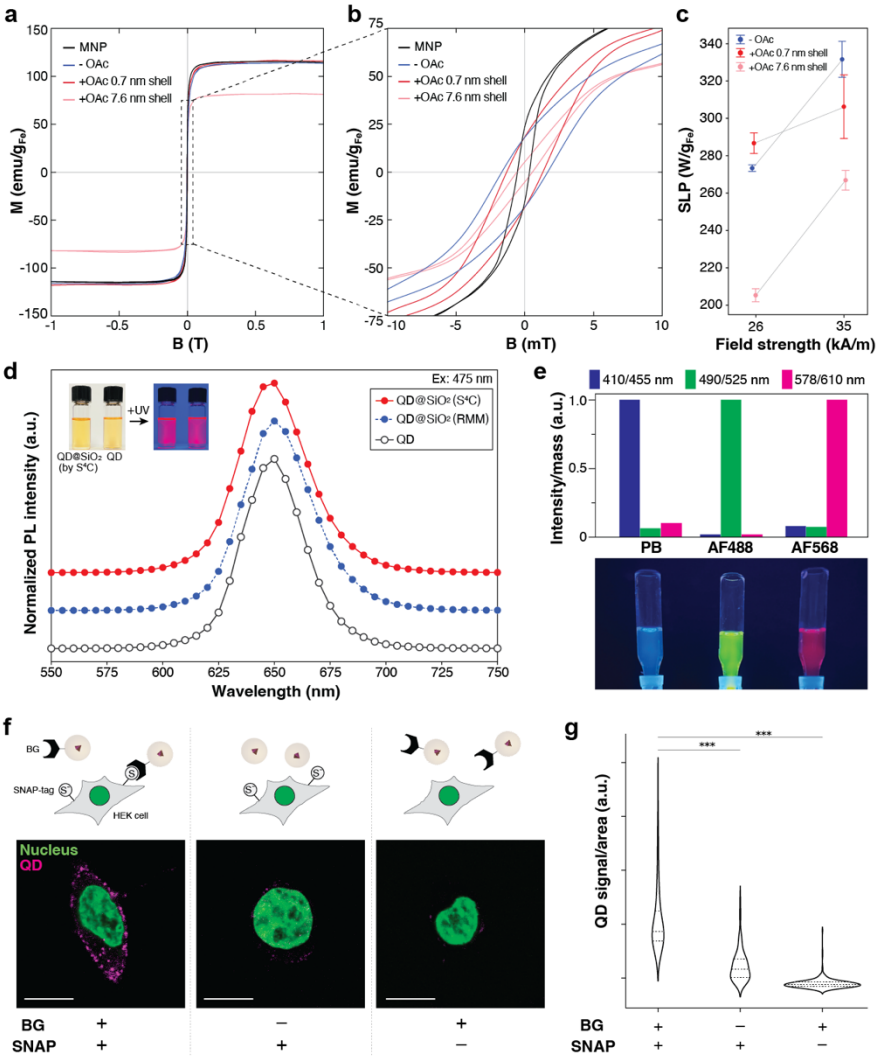

Figure 5. (a, b) Magnetization curves of bare MNPs and silica-coated MNPs. MNP: bare MNPs. -OAc: silica-coated MNPs by the conventional method. +OAc, 0.7 nm shell: silica-coated MNPs by SCHLR with shell thickness 0.7 nm. +OAc, 7.6 nm: silica-coated MNPs by SCHLR with shell thickness 7.6 nm. **(c)** SLP values of silica-coated MNPs. **(d)** Emission spectra of bare QD and silica-coated QD. The excitation wavelength was 475 nm. The concentration of QD is the same across the three conditions. The three plots are offset. **(e)** Fluorescence intensities of dye-labeled silica-coated MNP. The values were normalized by the mass of core MNPs. An image of corresponding dye-labelled MNPs under UV light is provided beneath the bar plot. **(f)** Fluorescence images of HEK cells cultured with BG-functionalized QDs and control cells. The cell nuclei were stained with a green dye (BioTracker green). QDs were excited at 600 nm and imaged in the window of 625 – 655 nm. Scale bars are 10 μm. **(g)** Statistical analysis of the fluorescence intensity from the QDs normalized by cell area. The model used was the Kruskal-Wallis one-way ANOVA. (***P < 0.0001).

3. Conclusion

RMM is a widely used approach for coating hydrophobic nanomaterials with silica as a means of preventing chemical degradation, simplifying surface ligand engineering, facilitating transfer

into aqueous media, and improving biocompatibility. However, the sensitivity of RMM to reaction conditions often manifests in non-uniform shell thickness and aggregation of particles during coating. Here we have demonstrated that the addition of hydrophobic ligand, OAc, to the reaction solution for RMM prevents the formation of multi-core particles, thereby enhancing the uniformity and reproducibility of silica shells. We have also shown that our modified silica coating protocol yields uniform silica shells of tunable thickness, including thin shells (<1 nm) that minimize alterations to overall particle size, shape, and functional properties (**Fig. 3, 5**). While the exact role of OAc in SCHLR will benefit from further study, our results indicate that the means by which OAc improves the RMM method is correlated to the manner in which it alters the composition of the particle ligand coating during the silica deposition. **(Fig. 1e**). We also hypothesize that additional OAc slows down the ligand exchange between TEOS and OAc, leading to higher concentration of hydrolyzed TEOS molecules in reverse micelles and enhancing the electrostatic screening effect.

The SCHLR method can be used to silica-coat nanomaterials with different core compositions (e.g. magnetite MNPs and CdSe/ZnS QDs), sizes (11-240 nm), and shapes (e.g. spheres vs. discs). Additionally, the SCHLR silica shells can be readily modified with a variety of moieties through established silica functionalization chemistries, enabling their use in, for example, biomedical applications. The only requisite for SCHLR is the initial nanoparticle passivation with OAc. However, many synthetic protocols for high-quality nanomaterials (MNPs, QDs) are conducted in hydrophobic organic solvents and use OAc as a primary surfactant, indicating potentially broad utility of this approach. We anticipate that silica-coated particles produced via the SCHLR method will empower colloidal nanomaterials research by offering enhanced reproducibility and control over particles' surface properties.

4. Experimental Section

All materials were purchased from Sigma-Aldrich unless otherwise mentioned and used as received.

Magnetic nanoparticle synthesis:

Magnetic nanoparticles (MNPs) of Fe_3O_4 (magnetite) were synthesized using the thermal decomposition method.[40] As a precursor, iron oleate was synthesized from sodium oleate and $FeCl_3 \cdot 6H_2O$.[35] 123 mmol of sodium oleate (TCI Chemicals) and 40 mmol $FeCl_3 \cdot 6H_2O$ were heated in a 250-mL three-neck flask in a 70 ºC oil bath in a mixture of 100 mL hexane, 50 mL ethanol, and 50 mL DI water for 90 min under N_2. The produced black liquid containing iron oleate was washed with ethanol and DI water 5 times in a separatory funnel to remove impurities, then dried at 110 ºC in an oil bath under vacuum overnight to remove remaining hexane, ethanol, and water. Dried iron oleate is a black, viscous solution that is stored under vacuum.

For MNP synthesis, 3 mmol of iron oleate was placed in a 250-mL three-neck flask and mixed with 6 mL of 1-octadecene, 3 mL of benzyl ether, and oleic acid. To control the size of MNPs, the amount of oleic acid was adjusted.[40] For 24 nm MNPs, 6 mmol of oleic acid was added. The mixture was degassed at 90 ºC under vacuum for 30 min, then heated at 330 ºC under N_2 for 30 min after it reached the reflux point. After cooling, synthesized MNPs were purified by centrifuge in a mixture of ethanol and hexane (ethanol : hexane = 1 : 4 (volume ratio)) three times. Washed MNPs were resuspended in 3 mL of chloroform and stored at 4 ºC.

Magnetic nanodisc synthesis: Magnetic nanodiscs (MNDs) were synthesized according to Gregurec *et al.*[41] Non-magnetic hematite nanodiscs (NDs) were synthesized using the hydrothermal method. 800 mg of sodium acetate and 273 mg of $FeCl_3 \cdot 6H_2O$ were placed in a Teflon vessel. After 10 mL of ethanol and 800 µL of DI water were added, the Teflon vessel was sealed tightly and heated at 180 ºC for 18 hours. The synthesized red solution was washed

with ethanol 3 times by centrifuge, and then the pellet of hematite NDs was resuspended in 5 mL of ethanol.

100 mg of the hematite NDs were placed in a 250-mL three-neck flask with 2.22 mL of oleic acid and 29 mL of trioctylamine. The solution was heated at 370 ºC with H_2 bubbling. Heating was stopped once the color of the solution changed from red to black. The black magnetite NDs (MNDs) were washed with a 1:1 mixture of hexane and ethanol two times and with chloroform three times using magnetic separation. MNDs were resuspended in 1 mL of chloroform and stored at 4º C.

Silica shell formation on nanomaterials through SCHLR and amine functionalization:

[*MNP*] The SCHLR method was developed based on RMM.[19] 25 mL of cyclohexane was placed in a 50-mL falcon tube. In the standard condition, 250 µL of oleic acid and 1540 mg of Igepal CO-520 were added to the tube and shaken to mix. 900 pmol of MNP in chloroform (typically less than 100 µL) was added and mixed well by vortexing. 210 µL of NH_4OH was added to the solution and mixed immediately. To control the thickness of the silica shell, the amount of tetraethyl orthosilicate (TEOS) was adjusted. For a 4 nm-thick silica shell, 4 µL of TEOS was added, followed by vortexing for 48 h. For amine functionalization, 1 µL of [3-(2-aminoethylamino)propyl]trimethoxysilane (AEAPTMS) was added to the solution and vortexed another 90 min.

To stop the reaction and purify the silica-coated MNPs, 4 mL of 50 mM tetramethylammonium hydroxide (TMAOH) in methanol was added to the tube. The tube was shaken for 5 sec and allowed to stand for 30 sec, and the black bottom layer was collected in another 50-mL tube and centrifuged at 10 kg for 10 min. After the supernatant was removed, the pellet was resuspended in 4 mL of the same TMAOH solution, and the solution was centrifuged at 10 kg for 10 min. The pellet was resuspended in 1 mL of dimethyl sulfoxide (DMSO) and sonicated, then centrifuged at 20 kg for 20 min. Repeat this DMSO washing step one more time. The final pellet was resuspended in 400 µL of DMSO and stored at room temperature.

[*Quantum dot*] Quantum dots (QDs) were purchased from Sigma-Aldrich (#919136, 11.5 nm, 5 mg/mL). For silica shell coating of QDs, the same recipe as silica-coated MNPs was applied except for the amount of QDs and TEOS. Typically, 100 µL of QD solution at 5 mg/mL in toluene was added to the reaction solution instead of MNPs. To obtain ~32 nm silica-coated QDs, 6 µL of TEOS was added.

[*MND*] The recipe for MNDs is the same as the one for MNPs except for the amount of MNDs and TEOS. Instead of MNPs, 2 mg of MNDs in chloroform was added to the reaction solution. 20 µL of TEOS (3.6 mM) was added to obtain ~4 nm-thick silica shells.

Functionalization of amine-functionalized silica shells through carbodiimide chemistry:

Amine-functionalized silica shells were modified with dyes (Pacific Blue-*N*-Hydroxysuccinimide (PB-NHS): Fluoroprobes #1245-5, Alexa Fluor 488 (AF488)-NHS and Alexa Fluor 568 (AF568)-NHS: Lumiprobe, #11820 and #14820, respectively), methoxy poly(ethylene glycol) (mPEG24-NHS; BroadPharm #BP-23970) or O^6-benzylguanine (BG)-PEG5k-NHS through NHS chemistry. BG-PEG5k-NHS was synthesized via NHS chemistry between BG-NH_2 (AmBeed #A455042) and NHS-PEG5k-NHS (Nanocs, #PG2-THTZ-5k).[42] 1 equivalent amount of NHS-PEG5k-PEG was mixed with 1.5 equivalent amount of BG-NH_2 in DMSO for 18 h. For all types of silica-coated nanomaterials, ligand density of 1 ligand/nm^2 was assumed and 20x equivalent of the number of ligands were used for NHS chemistry. The particles and ligands were mixed in DMSO on a vortex for 48 hours. The functionalized silica-coated nanomaterials were purified in DI water by 3 rounds of centrifugation at 20 kg for 20 min and stored at 4 ºC.

Structural and magnetic characterization:

Transmission electron microscope (TEM) images and electron diffraction patterns of all coated/non-coated nanomaterials were obtained with an FEI Tecnai G2 Spirit TWIN TEM. Fiji

was used for visualization and size analysis.[43] Dynamic light scattering measurements were performed with a Nicomp Nano DLS/ZLS systems. The concentration of nanomaterials was measured by using an Agilent 5100 Inductively Coupled Plasma-Optical Emission Spectrometer (ICP-OES). Room-temperature hysteresis loops were measured by a vibrating sample magnetometer (VSM, Digital Measurement Systems Model 880A).

Specific loss power (SLP) was measured in a similar method to previously-described (**Fig. S6**).[44,45] Briefly, 50 µL of sample solutions in DI water (2 mg/mL, n = 3) were placed in small glass vial together with an optical fiber temperature probe (Omega HHTFO-101) and measured.[46] The air gap between the sample tube and the coil is ~4 cm. Alternating magnetic field was applied with a frequency f = 163 kHz and amplitude H_0 = 35 kA/m. The field amplitude was measured using an inductive pick-up coil installed next to the main coil. As a control measurement, 50 µL of de-ionized (DI) water without MNPs was used, and no temperature change was observed.

Optical characterization of quantum dots:

Optical properties of QDs were measured with a Molecular Devices SpectaMax M2e with using a quartz cuvette. For photoluminescence measurements, excitation wavelength of 475 nm was used. For evaluation of the quantum yield, rhodamine B was used as a standard dye, which has the quantum yield of 0.36 in DI water.[47] The excitation and emission wavelengths for rhodamine B were 565 nm and 590 nm, respectively.

In vitro genetic cell targeting:

12-mm round coverslips (Electron Microscopy Sciences, #72196-12, #1 thickness) were coated with Matrigel (Corning) at a 1:30 dilution by the standard thin coating method provided by the manufacturer and placed in a 24-well plate. HEK293T cells were seeded on the coverslips in 1mL of Dulbecco's Modified Eagle Medium (DMEM, GlutaMAX supplement, Gibco) with

2.5% fetal bovine serum (FBS, Cytiva) and transfected when cells reach 70% confluency by adding a mixture of 4 µL of Lipofectamine 2000 (Invitrogen) and 1 µg of DNA plasmid (*pAAV-CMV::SNAPtm*) in 50 µL of Opti-MEM (Gibco). HEK cells were cultured at 37ºC with 5% CO_2. Media was exchanged for fresh media 6 hours after transfection. 48 hours after transfection, 2 µg of either QD-PEG/BG or QD-PEG in DI water was added to the medium. After incubation with QDs for 15 min, cells were washed with phosphate-buffered saline (PBS) 2 times and then fixed for 15 min in 4% paraformaldehyde in PBS. After three washes with PBS, cells were stained with BioTracker 488 (Sigma-Aldrich) in a 1:1000 dilution in PBS for 15 min. After three washes with PBS, coverslips were mounted onto glass slides using Fluoromount-G (Invitrogen).

Targeting specificity of QD-PEG/BG was evaluated and quantified using a Leica DMI8 Inverted Confocal Microscope. For quantification, a 20x objective lens was used to obtain fluorescence images. For high magnification images, a 60x objective lens was used. QDs were excited with a 400-nm diode laser and detected at 620-660 nm. The images were quantified by using CellProfiler.[48]

Nanomagnetic simulations:

Nanomagnetic Simulations were performed using MuMax3.[49] Particles were 24 nm spheres with edge to edge spacing of 2 nm (from TEM, **Fig. 2b**). The spheres had magnetic properties of magnetite: 110 emu/g-Fe (from VSM) and exchange constant = 1.3×10^{-12} J/m.[50] Hysteresis measurements were performed by slightly varying the applied external field and allowing the simulation to relax to its lowest energy state.

Supporting Information

All data needed to evaluate the conclusions in the paper are present in the manuscript or the supplementary materials. Reasonable quantities of physical samples of the described nanomaterials are available upon request.

Acknowledgements

The authors are grateful to T. Hueckel and G. Desroches for their technical advice on the experiments and manuscript preparation. This work was funded in part by the Pioneer Award from the National Institutes of Health and National Institute for Complementary and Integrative Health (DP1-AT011991, P.A.), NIH BRAIN Initiative and the National Institute for Neurological Disorders and Stroke (R01-NS115576, P. A.), McGovern Institute for Brain Research at MIT, and K. Lisa Yang and Hock E. Tan Center for Molecular Therapeutics at MIT (P.A.). R.J.M. acknowledges support from the Army Research Office under award W911NF-23-2-0101. K.N. is a recipient of a scholarship from the Honjo International Scholarship Foundation.

References

[1] M. A. Boles, D. Ling, T. Hyeon, D. V. Talapin, *Nature Mater* **2016**, *15*, 141.
[2] A. Heuer-Jungemann, N. Feliu, I. Bakaimi, M. Hamaly, A. Alkilany, I. Chakraborty, A. Masood, M. F. Casula, A. Kostopoulou, E. Oh, K. Susumu, M. H. Stewart, I. L. Medintz, E. Stratakis, W. J. Parak, A. G. Kanaras, *Chem. Rev.* **2019**, *119*, 4819.
[3] C. D. Walkey, J. B. Olsen, H. Guo, A. Emili, W. C. W. Chan, *J. Am. Chem. Soc.* **2012**, *134*, 2139.
[4] D. Bera, L. Qian, T.-K. Tseng, P. H. Holloway, *Materials* **2010**, *3*, 2260.
[5] E. C. Dreaden, A. M. Alkilany, X. Huang, C. J. Murphy, M. A. El-Sayed, *Chem. Soc. Rev.* **2012**, *41*, 2740.
[6] Y. Jun, Y.-M. Huh, J. Choi, J.-H. Lee, H.-T. Song, S. Kim, S. Yoon, K.-S. Kim, J.-S. Shin, J.-S. Suh, J. Cheon, *J. Am. Chem. Soc.* **2005**, *127*, 5732.
[7] J.-H. Lee, J. Jang, J. Choi, S. H. Moon, S. Noh, J. Kim, J.-G. Kim, I.-S. Kim, K. I. Park, J. Cheon, *Nature Nanotech* **2011**, *6*, 418.
[8] R. R. Arvizo, S. Bhattacharyya, R. A. Kudgus, K. Giri, R. Bhattacharya, P. Mukherjee, *Chem. Soc. Rev.* **2012**, *41*, 2943.
[9] S. Chinnathambi, N. Shirahata, *Science and Technology of Advanced Materials* **2019**, *20*, 337.
[10] R. Chen, G. Romero, M. G. Christiansen, A. Mohr, P. Anikeeva, *Science* **2015**, *347*, 1477.
[11] J. Lee, W. Shin, Y. Lim, J. Kim, W. R. Kim, H. Kim, J.-H. Lee, J. Cheon, *Nat. Mater.* **2021**, *20*, 1029.
[12] S. Chen, A. Z. Weitemier, X. Zeng, L. He, X. Wang, Y. Tao, A. J. Y. Huang, Y. Hashimotodani, M. Kano, H. Iwasaki, L. K. Parajuli, S. Okabe, D. B. L. Teh, A. H. All, I. Tsutsui-Kimura, K. F. Tanaka, X. Liu, T. J. McHugh, **2018**.
[13] Y.-W. Huang, M. Cambre, H.-J. Lee, *IJMS* **2017**, *18*, 2702.
[14] A. C. Marques, P. J. Costa, S. Velho, M. H. Amaral, *Journal of Controlled Release* **2020**, *320*, 180.
[15] M. J. Mitchell, M. M. Billingsley, R. M. Haley, M. E. Wechsler, N. A. Peppas, R. Langer, *Nat Rev Drug Discov* **2021**, *20*, 101.
[16] R. Abdul Jalil, Y. Zhang, *Biomaterials* **2008**, *29*, 4122.
[17] M. A. Malvindi, V. De Matteis, A. Galeone, V. Brunetti, G. C. Anyfantis, A. Athanassiou, R. Cingolani, P. P. Pompa, *PLoS ONE* **2014**, *9*, e85835.
[18] A. T. Heitsch, D. K. Smith, R. N. Patel, D. Ress, B. A. Korgel, *Journal of Solid State Chemistry* **2008**, *181*, 1590.
[19] J. Kim, D. Seo, J. Lee, K. M. Southard, Y. Lim, D. Kim, Z. J. Gartner, Y. Jun, J. Cheon, *Nat Protoc* **2017**, *12*, 1871.
[20] V. V. Goftman, T. Aubert, D. V. Ginste, R. Van Deun, N. V. Beloglazova, Z. Hens, S. De Saeger, I. Yu. Goryacheva, *Biosensors and Bioelectronics* **2016**, *79*, 476.
[21] M. Darbandi, R. Thomann, T. Nann, *Chem. Mater.* **2005**, *17*, 5720.
[22] H. L. Ding, Y. X. Zhang, S. Wang, J. M. Xu, S. C. Xu, G. H. Li, *Chem. Mater.* **2012**, *24*, 4572.
[23] C. Vogt, M. S. Toprak, M. Muhammed, S. Laurent, J.-L. Bridot, R. N. Müller, *J Nanopart Res* **2010**, *12*, 1137.
[24] E.-S. Jang, *Journal of the Korean Chemical Society* **2012**, *56*, 478.
[25] R. Koole, M. M. van Schooneveld, J. Hilhorst, C. de Mello Donegá, D. C. 't Hart, A. van Blaaderen, D. Vanmaekelbergh, A. Meijerink, *Chem. Mater.* **2008**, *20*, 2503.
[26] R. Chen, M. G. Christiansen, P. Anikeeva, *ACS Nano* **2013**, *7*, 8990.
[27] J. Park, K. An, Y. Hwang, J.-G. Park, H.-J. Noh, J.-Y. Kim, J.-H. Park, N.-M. Hwang, T. Hyeon, *Nature Mater* **2004**, *3*, 891.

[28] E. Ureña-Horno, M.-E. Kyriazi, A. G. Kanaras, *Nanoscale Adv.* **2021**, *3*, 3522.
[29] Y. Zhu, F. Y. Jiang, K. Chen, F. Kang, Z. K. Tang, *J Sol-Gel Sci Technol* **2013**, *66*, 180.
[30] D. C. Lee, F. V. Mikulec, J. M. Pelaez, B. Koo, B. A. Korgel, *J. Phys. Chem. B* **2006**, *110*, 11160.
[31] Y. Yang, L. Jing, X. Yu, D. Yan, M. Gao, *Chem. Mater.* **2007**, *19*, 4123.
[32] K. Kittipongpittaya, A. Panya, D. J. McClements, E. A. Decker, *J Americ Oil Chem Soc* **2014**, *91*, 453.
[33] W. Chaiyasit, C. B. Stanley, H. H. Strey, D. J. McClements, E. A. Decker, *Food Biophysics* **2007**, *2*, 57.
[34] S. Sugiura, S. Ichikawa, Y. Sano, M. Nakajima, X. Q. Liu, M. Seki, S. Furusaki, *Journal of Colloid and Interface Science* **2001**, *240*, 566.
[35] J. Moon, M. G. Christiansen, S. Rao, C. Marcus, D. C. Bono, D. Rosenfeld, D. Gregurec, G. Varnavides, P. Chiang, S. Park, P. Anikeeva, *Adv. Funct. Mater.* **2020**, *30*, 2000577.
[36] F. J. Arriagada, K. Osseo-Asare, *Colloids and Surfaces A: Physicochemical and Engineering Aspects* **1999**, *154*, 311.
[37] R. Hergt, S. Dutz, R. Müller, M. Zeisberger, *J. Phys.: Condens. Matter* **2006**, *18*, S2919.
[38] J. Carrey, B. Mehdaoui, M. Respaud, *Journal of Applied Physics* **2011**, *109*, 083921.
[39] A. Keppler, S. Gendreizig, T. Gronemeyer, H. Pick, H. Vogel, K. Johnsson, *Nat Biotechnol* **2003**, *21*, 86.
[40] R. Chen, M. G. Christiansen, A. Sourakov, A. Mohr, Y. Matsumoto, S. Okada, A. Jasanoff, P. Anikeeva, *Nano Lett.* **2016**, *16*, 1345.
[41] D. Gregurec, A. W. Senko, A. Chuvilin, P. D. Reddy, A. Sankararaman, D. Rosenfeld, P.-H. Chiang, F. Garcia, I. Tafel, G. Varnavides, E. Ciocan, P. Anikeeva, *ACS Nano* **2020**, *14*, 8036.
[42] S. M. Wichner, V. R. Mann, A. S. Powers, M. A. Segal, M. Mir, J. N. Bandaria, M. A. DeWitt, X. Darzacq, A. Yildiz, B. E. Cohen, *ACS Nano* **2017**, *11*, 6773.
[43] J. Schindelin, I. Arganda-Carreras, E. Frise, V. Kaynig, M. Longair, T. Pietzsch, S. Preibisch, C. Rueden, S. Saalfeld, B. Schmid, J.-Y. Tinevez, D. J. White, V. Hartenstein, K. Eliceiri, P. Tomancak, A. Cardona, *Nat Methods* **2012**, *9*, 676.
[44] D. Rosenfeld, A. W. Senko, J. Moon, I. Yick, G. Varnavides, D. Gregureć, F. Koehler, P.-H. Chiang, M. G. Christiansen, L. Y. Maeng, A. S. Widge, P. Anikeeva, *Sci. Adv.* **2020**, *6*, eaaz3734.
[45] M. G. Christiansen, C. M. Howe, D. C. Bono, D. J. Perreault, P. Anikeeva, *Review of Scientific Instruments* **2017**, *88*, 084301.
[46] D. Rosenfeld, H. Field, Y. J. Kim, K. K. L. Pang, K. Nagao, F. Koehler, P. Anikeeva, *Adv Funct Materials* **2022**, *32*, 0224558.
[47] X.-F. Zhang, Y. Zhang, L. Liu, *Journal of Luminescence* **2014**, *145*, 448.
[48] D. R. Stirling, M. J. Swain-Bowden, A. M. Lucas, A. E. Carpenter, B. A. Cimini, A. Goodman, *BMC Bioinformatics* **2021**, *22*, 433.
[49] A. Vansteenkiste, J. Leliaert, M. Dvornik, M. Helsen, F. Garcia-Sanchez, B. Van Waeyenberge, *AIP Advances* **2014**, *4*, 107133.
[50] G. Lavorato, E. Winkler, B. Rivas-Murias, F. Rivadulla, *Phys. Rev. B* **2016**, *94*, 054405.